International Journal of Biological Macromolecules 280 (2024) 135671

Contents lists available at ScienceDirect

International Journal of Biological Macromolecules

journal homepage: www.elsevier.com/locate/ijbiomac

CgLS mediates limonene synthesis of main essential oil component in secretory cavity cells of *Citrus grandis* 'Tomentosa' fruits

Ning Rong [a,c,d,e], Liying Huang [a,c,d,e], Peng Ye [a,c,d,e], Huimin Pan [a,c,d,e], Mingli Hu [f], Mei Bai [a,b,c,d,e,*], Hong Wu [a,c,d,e,*]

[a] *Guangdong Laboratory for Lingnan Modern Agriculture, South China Agricultural University, Wushan Road, Guangzhou 510642, China*
[b] *Maoming Branch, Guangdong Laboratory for Lingnan Modern Agriculture, Youchenliu Road, Maoming 525000, China*
[c] *Guangdong Technology Research Center for Traditional Chinese Veterinary Medicine and Natural Medicine, South China Agricultural University, Wushan Road, Guangzhou 510642, China*
[d] *Guangdong Key Laboratory for Innovative Developmentand Utilization of Forest Plant Germplasm, South China Agricultural University, Wushan Road, Guangzhou 510642, China*
[e] *Center for Medicinal Plants Research, College of Life Sciences, South China Agricultural University, Guangzhou 510642, China*
[f] *School of Pharmacy, Xianning Medical College, Hubei University of Science and Technology, Xianning 437100, China*

ARTICLE INFO

Keywords:
Citrus grandis 'Tomentosa'
Essential oil
Secretory cavity
Limonene synthase
Limonene

ABSTRACT

D-Limonene is the predominant component of essential oil from Exocarpium Citri Grandis, known for its antibacterial, antioxidant, insecticidal, and anti-inflammatory properties. The synthesis, transport, and accumulation of D-limonene in *Citrus grandis* 'Tomentosa' fruits are regulated by limonene synthase (LS) and its associated regulatory genes. This study addresses the gap in understanding the spatiotemporal cytological changes of LS and its regulatory genes. Through cytochemical techniques, we investigated the distribution of essential oil in the plastids, endoplasmic reticulum, and vacuoles of secretory cavity cells. We identified the LS-encoding gene *CgLS via* transcriptomics and demonstrated *in vitro* that CgLS catalyzes the formation of D-limonene from geranyl diphosphate (GPP). Transient overexpression of *CgLS* increased monoterpene limonene accumulation, while TRV virus-induced gene silencing reduced it. *CgLS* expression levels and D-limonene content showed spatiotemporal consistency with fruit development, with *in situ* hybridization revealing predominant expression in secretory cavity cells. Immunocytochemical localization indicated that CgLS is primarily located in the endoplasmic reticulum, plastids, and vacuoles. Our findings suggest that CgLS is translated in the endoplasmic reticulum and transported to plastids and vacuoles where D-limonene synthesis occurs. This study provides comprehensive insights into the characteristics of CgLS and its role in D-limonene synthesis at the tissue, cellular, and molecular levels in *C. grandis* 'Tomentosa'.

1. Introduction

Citrus peel essential oil (CPEO) is a complex mixture of aromatic compounds renowned for its health benefits [1–3]. The composition of CPEO is highly intricate, predominantly consisting of terpenoids, acids, aldehydes, and esters, with monoterpene limonene being the most abundant, accounting for 55.4 % to 91.7 % of CPEO [3–6]. Limonene exhibits various pharmacological activities, including antioxidant [7], anti-inflammatory [7–9], antibacterial [9], anticancer [10], and neuroprotective effects [10], making CPEO valuable in the pharmaceutical industry [11]. Additionally, CPEO's pleasant lemon fragrance finds application as a flavoring agent in food products and as a fragrance ingredient in cosmetics [12].

Essential oils are primarily stored in the secretory structures of plants [13]. Early cytological studies suggested their production in the cytoplasm [14] and plastids [15], while advanced terpenoid anabolism studies identified the mevalonate (MVA) and methylerythritol phosphate (MEP) pathways in the cytoplasm and plastids, respectively, as

* Corresponding authors at: Guangdong Laboratory for Lingnan Modern Agriculture, South China Agricultural University, Wushan Road, Guangzhou 510642, China.
E-mail addresses: baimei924@scau.edu.cn (M. Bai), wh@scau.edu.cn (H. Wu).

https://doi.org/10.1016/j.ijbiomac.2024.135671
Received 5 June 2024; Received in revised form 9 September 2024; Accepted 13 September 2024
Available online 14 September 2024

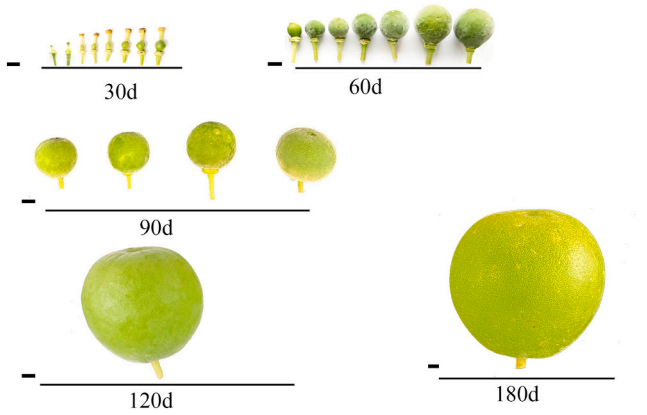

Fig. 1. Morphology of *C. grandis* 'Tomentosa'e fruit at different stages. d: after flowering; bar = 1 cm.

key synthesis routes [16–18]. These pathways produce isopentenyl diphosphate (IPP) and dimethylallyl pyrophosphate (DMAPP), which are further catalyzed by geranyl diphosphate synthase (GPPS) and geranylgeranyl diphosphate synthase (GGPPS) to form geranyl diphosphate (GPP), farnesyl diphosphate (FPP), and geranylgeranyl diphosphate (GGPP) [19]. GPP and FPP serve as direct precursors for monoterpene and sesquiterpene biosynthesis, catalyzed by terpene synthase [20].

In *Catharanthus roseus*, *Litsea cubeba*, and *Chimonanthus praecox*, GPPS/GGPPS has been subcellularly localized to the plastids [21–24]. However, it was also compartmentalized in the mitochondria, cytoplasm, and endoplasmic reticulum [25]. In Citrus species such as *C. limon*, *C. unshiu*, and *C. sinensis*, monoterpene synthase genes have been cloned and characterized [26–28]. Recently, several limonene synthase (LS) genes (*FcLSs*) were identified in *Fortunella crassifolia*, of which 18 exhibited 12 single nucleotide polymorphisms in the open reading frame (ORF), resulting in variations in the FcLS protein [6]. Labeling of immunogold particles with polyclonal antibodies against LS has specifically localized it to plastids [29]. These studies have provided significant theoretical and technical data for further investigations into the synthesis, transport, and storage of terpenes in citrus plants.

Exocarpium Citri Grandis (ECG) is a traditional Chinese medicine derived from the immature or nearly mature dried exocarps of *C. grandis* 'Tomentosa' fruits, which has been utilized as a therapeutic agent for over 1500 years [30,31]. ECG is rich in bioactive compounds, including flavonoids, polysaccharides, and essential oils [31]. Among these components, with limonene being extensively studied for its pharmacological activity [32–35]. Despite the cloning and identification of several LS genes in citrus plants [6,26–28], data on the spatiotemporal cytological changes of LS and its related regulatory genes remain scarce, limiting the functional analysis of LS.

This study comprehensively examines the synthesis, transport, and accumulation of essential oil during the development of secretory cavities in *C. grandis* 'Tomentosa' fruits. Through transcriptional analysis, *CgLS* was identified as a putative LS-encoding gene. *In vitro* and *in vivo* experiments confirmed the role of CgLS in D-limonene synthesis. *In situ* hybridization and immunocytochemical techniques revealed that *CgLS* was predominantly expressed in secretory cavity cells, with significant protein concentrations in the endoplasmic reticulum, plastids, and vacuoles. These findings indicate the crucial role of CgLS in D-limonene biosynthesis in *C. grandis* 'Tomentosa' fruits.

This study thoroughly investigates the synthesis, transport, and accumulation of essential oils in the developing secretory cavities of *C. grandis* 'Tomentosa' fruits. Through transcriptional analysis, CgLS was identified as a candidate gene encoding limonene synthase. *In vitro* and *in vivo* experiments validated the role of CgLS in the synthesis of D-limonene, a key monoterpene. *In situ* hybridization and immunocytochemical techniques revealed that CgLS is predominantly expressed in secretory cavity cells, with significant localization in the endoplasmic reticulum, plastids, and vacuoles. These findings underscore the pivotal role of CgLS in D-limonene biosynthesis, highlighting its potential impact on the production of bioactive compounds in *C. grandis* 'Tomentosa' fruits. This study aims to advance the understanding of the biochemical pathways and regulatory mechanisms governing essential oil biosynthesis in medicinal plants, providing a valuable contribution to the fields of natural product research and biotechnology.

2. Materials and methods

2.1. Materials

The plant materials utilized in this investigation were collected from Ligang Town, Huazhou City, Guangdong Province (21°47′4″N, 110°38′29″E). Fruits were harvested at different developmental stages: 30, 60, 90, 120, and 180 days after flowering (DAF) (Fig. 1). Immediately upon collection, the ovary wall and exocarp were flash-frozen in liquid nitrogen and stored at −80 °C. The remaining portions were fixed in a specific solution for further processing.

2.2. Semi-thin sectioning

Following the methodology described by Bai et al. [36], the fruits were segmented into cubes measuring 5 × 5 × 5 mm. The cubes were promptly immersed in a fixing solution consisting of 3 % paraformaldehyde and 2 % glutaraldehyde, and fixed overnight at 4 °C. Subsequently, they were rinsed thrice with 0.1 M PBS for 15 min each. The samples were then treated with 1 % osmium acid at room temperature for 2 h and rinsed again thrice with 0.1 M PBS for 15 min each. They were dehydrated using an ethanol gradient (30 %, 45 %, 60 %, 70 %, 80 %, 90 %, and 100 %), permeated with propylene oxide, and embedded in Epon812 resin (SPI Supplies, West Chester, PA, USA). Finally, the cubes were sliced into 2 μm thick sections using an RM2155 thin microslicer (Leica, Wetzlar, Hesse-Darmstadt, Germany), stained with 0.1 % toluidine blue, and observed under a DM6B microscope (Leica, Germany).

2.3. Ultrathin section and immunocytochemical localization

The semi-thin sections were further sliced into 70–90 nm thick ultrathin sections using an EM UC7 microtome (Leica, Germany). These sections were placed on copper or nickel meshes covered with formvar film. A copper mesh was employed for routine electron microscopy, while a nickel mesh was utilized for immunocytochemical localization. The nickel mesh with the sample was treated with 8 % sodium periodate for 4 min and washed thrice with ddH_2O and PBST (10 mM PBS, 0.02 % Tween-20, 0.15 M NaCl) for 5 min each. The mesh was then incubated in PBG (0.2 M glycine, 1 % BSA in PBS-T) for 40 min, followed by washing with PBS-T thrice for 5 min each. The mesh was incubated with anti-CgLS polyclonal primary antibodies in PBA (1 % BSA in PBST) at a ratio of 1: 9 (*v*/v) and incubated at 37 °C for 2 h. The anti-CgLS antibodies were previously extracted and purified as described by Bai et al [36] Next, the mesh was washed with PBS-T seven times for 5 min each, incubated with PBA containing secondary antibody at a ratio of 1:50 (v/v) immobilized on 10 nm colloidal gold particles, and incubated at 37 °C for 1 h. Subsequently, it was washed with PBS-T seven times for 5 min each, followed by five washes with ddH_2O for 5 min each. The copper or nickel mesh containing the sections was stained with a uranium dioxyacetate solution for 15 min, washed with ddH_2O ten times, and stained with lead citrate solution for 25 min. After washing, the sections were dried at 37 °C and observed under a Talos L120C transmission electron microscope (Thermo-Fisher Scientific, Waltham, MA, USA). Control samples were treated similarly, with specific antibodies replaced by pre-immunized serum (control A) or PBS-T (control B).

2.4. Immunohistochemistry

The fruits of *C. grandis* 'Tomentosa' were cut into small pieces and fixed in 4 % paraformaldehyde. Subsequently, they were dehydrated through a graded series of alcohols, cleared with xylene, infiltrated with paraffin, and embedded. After trimming, 5 μm thick sections were prepared using a Reichert Histo STAT 820 paraffin microtome. The paraffin sections were deparaffinized and rehydrated, followed by three washes with PBS (0.01 M, pH 7.2). The sections were then blocked with blocking solution for 30 min, incubated with diluted primary antibodies overnight at 4 °C, washed three times with PBS, incubated with diluted secondary antibodies for 1 h at room temperature, and washed three times with PBS. The sections were observed under a DM6B microscope (Leica, Germany).

2.5. Subcellular localization

The full-length *CgLS* gene was amplified by PCR and cloned into the 35S-eGFP vector. The recombinant plasmid was then transferred into *Agrobacterium tumefaciens* strain GV3101 by electroporation. The bacterial culture was collected by centrifugation and resuspended in infiltration buffer (10 mM MES, 10 mM $MgCl_2$, 150 μM acetosyringone, pH 5.6) to an OD600 nm of 0.75. The prepared buffer was infiltrated into the undersides of the leaves of 4-week-old *Nicotiana benthamiana* plants using a 1 mL needleless syringe. Two days post-transformation, the fluorescence was observed under a DM6B microscope (Leica, Germany).

2.6. RNA extraction and real-time quantitative PCR (qRT-PCR) analysis

Total RNA from the exocarps of *C. grandis* 'Tomentosa' fruits at different developmental stages was extracted using the Rapid Universal Plant RNA Extraction Kit 3.0 (Beijing Huachioyang Biotechnology Co., Ltd., Beijing, China). RNA concentration was measured using a Nanodrop™ 2000 (Thermo-Fisher Scientific), and quality was assessed using agarose gel electrophoresis. Genomic DNA contamination was removed using the PrimeScript™ RT Reagent Kit with gDNA Eraser (Perfect Real Time) (TaKaRa, Beijing, China), and the first-strand cDNA was synthesized using 1 μg RNA in a reaction volume of 20 μL.

Based on genomic and transcriptomic data previously published by our group [37], an LS-encoding gene, *CgLS*, was identified. qRT-PCR was employed to analyze *CgLS* expression using *β-actin* as an internal control in three independent biological replicates. The primer sequences used are provided in Table S1.

2.7. Cloning and sequence analysis of CgLS gene

The total RNA and cDNA synthesis methods were described in the previous section. *CgLS* ORF-specific primers were designed using the NCBI Primer Blast tool (https://www.ncbi.nlm.nih.gov/tools/primer-blast/). Detailed primer information is available in Table S1. *CgLS* was translated using the DNAMAN8.0 software (https://www.lynnon.com/). The MEGA X (64-bit) software (https://www.megasoftware.net/) was used for sequence alignment and phylogenetic tree construction. The InterPro database (https://www.ebi.ac.uk/interpro/) was employed to predict the functional domain of the protein.

2.8. In situ hybridization

In situ hybridization of the paraffin tissue sections was performed following the method described by Bai et al [36] The sequence of the probe used was: TGCATTAATCCCTCAACCTTGGTTACCTCTGTAAATGGTTTCAAATGTCTTCCTCTTGCAACAAATAAAGCAGCGATCAGAATCATGGCAAAAAATAAGCCAGTCCAATGCCTTGTCAACGCCAAATATGATAATTTGACAGTTGATAGGAGATCAGCAAACTACCAACCTTCAATTTGGGACCATGATTTTTTGCAGTCATTGAATAGCAACTATACGGATGAAACATACAGAAGACGAG. Hybridization signals were observed and photographed under a DM6B microscope (Leica, Germany).

2.9. Extraction and gas chromatography–mass spectrometry (GC–MS) determination of volatile components

Using the method described by Li et al. [38], fruits at different stages of development were ground into fine powder and ~ 150 mg of it was weighed and placed into a brown bottle. Then, 1.5 mL of hexane was added, and the mixture was subjected to ultrasound treatment for 30 min and centrifuged at 12,000 rpm for 30 min. The supernatant was collected, filtered using a 0.22 μm organic filter membrane, and transferred to a sample bottle for GC–MS analysis.

GC–MS was conducted using a 7890B-5977B instrument (Agilent, Santa Clara, CA, USA) and a 30 mm × 0.25 mm × 0.25 μm gas column with helium as the carrier gas. Initially, the column was set at 40 °C for 3 min, then increased to 280 °C at a rate of 12 °C/min for 3 min, and finally maintained at 280 °C for 5 min. A sample size of 0.2 μL was injected. An EI source mass spectrum was utilized, and the terpenoid structures were determined using the NIST14 mass spectrum library and comparison with standards.

2.10. Expression and purification of CgLS protein and in vitro enzymatic reaction

The open reading frame (ORF) of *CgLS* was cloned into the pMAL-C5X vector using the ClonExpress Ultra One Step Cloning Kit (Vazyme Biotech Co., Ltd., Nanjing, China). Primers specified in Table S1 facilitated the cloning. Following verification by sequencing, the recombinant plasmid was expressed in *E. coli* Rosetta™ (DE3) competent cells. Induction of the MBP-CgLS fusion protein was achieved by adding 0.5 mM isopropyl-β-D-1-thiogalactopyranoside (IPTG) and incubating at 20 °C for 12–16 h. Cells were harvested by centrifugation at 7000 rpm for 10 min. The cell lysate was obtained by ultrasonic disruption for 15 min and then centrifuged at 10,000 rpm at 4 °C for 30 min to clarify. The supernatant was treated with buffer containing 1 mM $MgCl_2$ and 1 mM phenylmethylsulfonyl fluoride (PMSF). This mixture was applied to an MBP-tagged resin column, incubated at 4 °C for 1 h to facilitate binding, and washed twice with buffer. The target protein was eluted in 1 mL fractions of elution buffer, each incubated at 4 °C for 30 min. The purified protein was then concentrated using a 30 kDa ultrafiltration tube.

Enzymatic activity was assessed following the protocol by Wang et al [39] Native recombinant CgLS was tested with geranyl pyrophosphate (GPP) or farnesyl pyrophosphate (FPP) (Sigma-Aldrich, Burlington, MA, USA) as substrates, and boiled-denatured CgLS served as a negative control. A 100 μL reaction mixture containing 40 μg of purified protein and 1 μL of 1 mg/mL GPP or FPP was prepared in a buffer of 25 mM HEPES, 5 mM dithiothreitol (DTT), and 5 mM MgCl2 (pH 7.0). The reaction was sealed under 200 μL of hexane and incubated at 37 °C for 2 h. The reaction was terminated by vortexing for 5 min, followed by a 5-min incubation at room temperature. The mixture was centrifuged at 12,000 rpm for 5 min, and the upper organic phase was transferred to a sample vial for analysis by gas chromatography–mass spectrometry (GC–MS) [39], following the protocol described in Section 2.7.

2.11. Total plant protein extraction and Western blot

The exocarp from *C. grandis* 'Tomentosa' fruits at different developmental stages (30, 60, 90, 120, and 180 days) was processed for total protein extraction using a plant protein microextraction kit (Tienze, China). Protein concentrations were quantified by the Bradford method before storage at −80 °C. Proteins extracted from each developmental stage were separated using 10 % SDS-PAGE. After electrophoresis, the proteins were electrotransferred onto a PVDF membrane (Bio-Rad, Hercules, CA, USA) with a constant 200 mA current at 4 °C for 80 min. The membrane was incubated overnight with an anti-CgLS-specific polyclonal antibody (primary antibody, 1:1000 *v*/v) at 4 °C. The

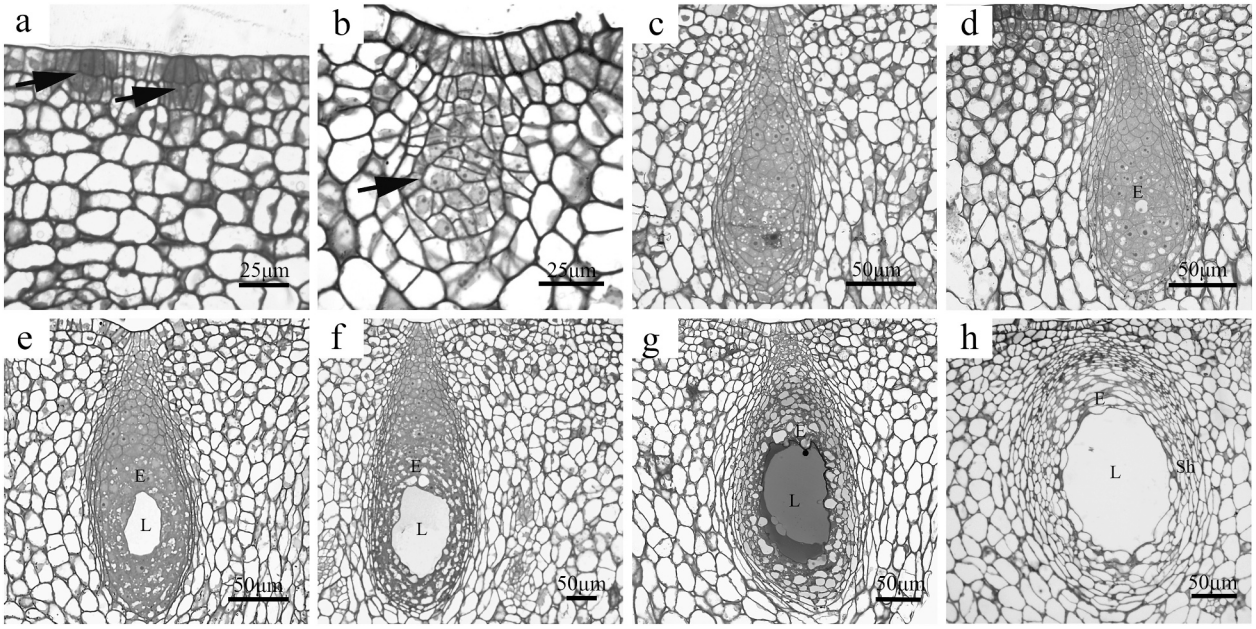

Fig. 2. Microstructure of secretory cavity development of *C. grandis* 'Tomentosa'e fruit.
a: The early stage of the initial cells of the secretory cavity (indicated by a black arrow).
b: The middle stage of the initial cells of the secretory cavity (indicated by a black arrow).
c: The late stage of the initial cells of the secretory cavity.
d: Intercellular formation stage.
e-f: The stage of lumen expansion.
e: The early stage of lumen expansion.
f: The middle stage of lumen expansion.
g: The late stage of lumen expansion.
h: Mature stage.
E: The epithelial cell.
L: The lumen of the secretory cavity.
Sh: The sheath cell.

following day, it was incubated with a peroxidase-linked secondary antibody, goat anti-rabbit IgG (H + L) (1:20,000 v/v) (Yeasen Biotechnology, Shanghai, China), at room temperature for 1 h. The membrane was then washed with PBST ten times, each for 6 min. For the detection of β-tubulin as a reference protein, a primary antibody (1:1000 v/v) and a secondary antibody, goat anti-mouse IgG (H + L) peroxidase-conjugated (1:5000 v/v) (both from Abmart Biotechnology, Shanghai, China), were used. Detection was completed using Super ECL Detection Reagent (Yeasen Biotechnology, Shanghai, China).

2.12. Transient overexpression of CgLS in C. grandis 'Tomentosa' leaves

Double enzyme cutting sites *Kpn*I and *Sal*I were designed on the pCAMBIA1300-HA vector for the construction of the recombinant plasmid. This plasmid was then transferred to *Agrobacterium tumefaciens* strain GV3101 by electroporation and cultured at 200 rpm and 28 °C until reaching an OD600 of 0.5–0.6. Simultaneously, *Agrobacterium* pSoup-p19 was also cultured. The bacteria were collected by centrifugation at room temperature for 5 min at 7000 rpm. An osmotic solution (10 mM MES, 150 μM acetosyringone, 10 mM MgCl2, ddH2O, pH 5.6) was added to suspend the bacteria and adjust the OD600 to 0.75. After standing at room temperature for 2 h, the *Agrobacterium* containing the CgLS target gene was mixed with p19 in equal volumes. To introduce the bacterial solution, a small incision was made on the back of the *C. grandis* 'Tomentosa' leaf using a needle. Subsequently, a 1 mL syringe without a needle was used to slowly inject the solution into the back of the leaf, ensuring it was completely filled with the bacterial solution. One side of the same leaf served as the empty control, while the other side was the experimental group with the *CgLS* gene [40]. Transient expression treatments were repeated three times with eight leaves each.

2.13. TRV-induced gene silencing (VIGS)

VIGS was performed based on a study with minor modification [41]. *Agrobacterium* cells expressing TRV1, TRV2, or TRV2-CgLS-derived vectors were cultured until an OD600 of 0.5–0.8 was reached. They were then collected by centrifugation and resuspended in an MES infiltrating buffer (200 μM acetylsyringone, 10 mM $MgCl_2$, and 10 mM MES; pH 5.6). The three vectors were mixed in a ratio of 1:1:1 (*v*/v) and incubated at room temperature for 3 h. Newly germinated saffron seedlings with a bud length of 1–2 cm were immersed in the *Agrobacterium* resuspension, placed in a vacuum container, and the air removed using a vacuum pump for 5 min. The stained area was washed with water and then replanted in the soil. For analysis, three biological replicates with ten seedlings each were sampled. After 28 days, the harvested material was used for gene expression assessment and GC–MS analysis following the methods described in Sections 2.4 and 2.7.

2.14. Data analysis

The data were initially processed using Excel 2010 (Microsoft Co., Redmond, WA, USA). GraphPad Prism 8 software (www.graphpad.com) was utilized for data visualization and variance analysis. For cases with fewer than three independent variables, a one-tailed *t*-test was employed. For cases with more than three independent variables, a one-way analysis of variance (ANOVA) followed by Duncan's multiple range test was used to ascertain the statistical significance of the differences.

3. Results

3.1. Dynamic changes in essential oil accumulation during the development of secretory cavities in C. grandis 'Tomentosa' fruit

Secretory cavities are common structures in citrus plants and serve as important sites for the production and accumulation of essential oil. Based on the morphological characteristics of secretory cavity cells, the development process of the secretory cavities can be divided into distinct stages: the initial cells stage, intercellular formation stage, lumen expansion stage, and mature stage (Fig. 2).

During the early stage of initial cells, a cluster of 8–10 closely arranged cells is formed in the epidermis and underlying layers. These cells exhibit dense cytoplasm, clear nucleoli (Fig. 2a), and a limited presence of black osmophilic droplets distributed within plastids and endoplasmic reticulum (Fig. 3a). Subsequently, these cells undergo uneven division, forming a cell mass comprising >30–40 cells, characterizing the middle stage of the initial cells (Fig. 2b). At this stage, a small number of black osmophilic droplets are observed within plastids and endoplasmic reticulum (Fig. 3b). In the late stage of the initial cells, the secretory cavity differentiates into a distinctive cap region and a global region. The cap region cells are flat and located outside the global region, which represents the future cavity formation site. The central cells exhibit dense cytoplasm and distinct nuclei (Fig. 2c). Numerous osmophilic droplets are distributed on the vacuoles and plastids, with the transport of osmophilic droplets to the vacuoles being observed (Fig. 3c-f). When the central cells of the global region separate, forming a small space surrounded by 3–5 cells, this marks the intercellular formation stage. The 3–4 layers of cells surrounding this small space will develop into epithelial cells in the future (Fig. 2d). At this stage, a large number of osmophilic droplets are present in the cytoplasm and plastids (Fig. 3g-i), and a well-developed endoplasmic reticulum is distributed around the plastids (Fig. 3h). The cell wall of the first layer of epithelial cells surrounding the cavity forms a unique cup shape

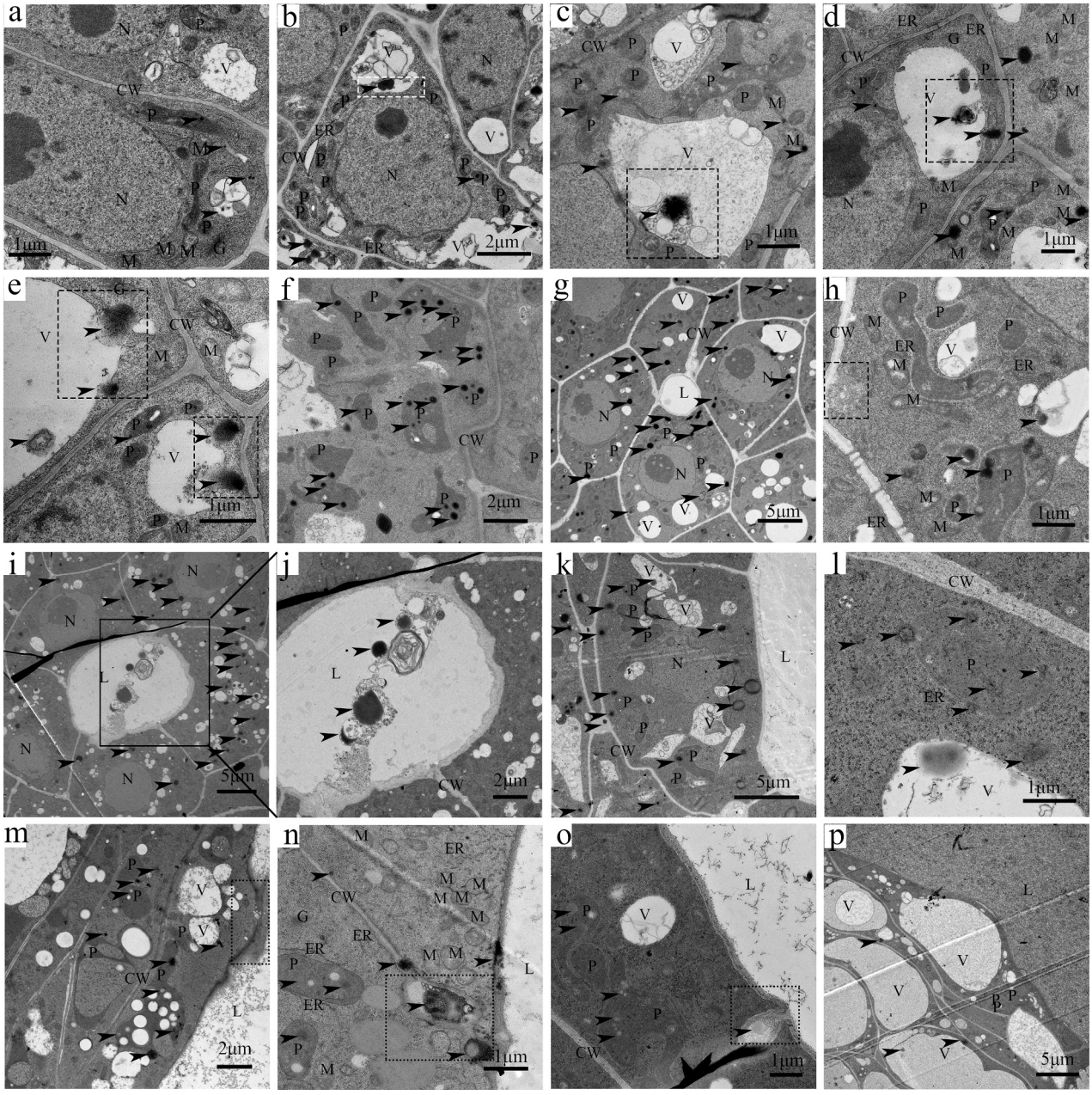

(caption on next page)

Fig. 3. Ultrastructure of secretory cavity development in *C. grandis* 'Tomentosa' fruits.
a: In the early stage of the initial cells, an abundance of plastids was observed, along with a meager quantity of black osmophilic droplets in the plastids and endoplasmic reticulum.
b: The middle stage of the initial cells reveals the presence of black osmophilic droplets in the plastids and the enlarged vesicles at the end of the endoplasmic reticulum (indicated by the white box).
c–f: During the late stage of the initial cells, black osmophilic droplets can be seen in the vacuole (indicated by the dotted black box) and transported from the cytoplasm. Additionally, an abundance of plastids with numerous osmophilic droplets was observed (f).
g–j: The intercellular formation stage is characterized by a high concentration of osmophilic droplets distributed in the plastids and the cytoplasm. Notably, "h" shows a marked accumulation of osmophilic droplets in the plastids and a well-developed endoplasmic reticulum. In "j," an enlarged image from "i," the first layer of epithelial cells in the secretory cavity was evident, which was concave and secreted black osmophilic droplets into the lumen.
k–o: The lumen expansion stage involves the release of gray osmophilic droplets from the plastid into the cytoplasm, which are then transported to the endoplasmic reticulum l: White vesicles initially appear on the wall of the lumen (indicated by the dotted line and black box) in "m" and subsequently diffuse into the lumen. In "n," cracks appear in the cell wall between the epithelial cells, accompanied by the distribution of a large number of gray osmophilic droplets (indicated by the dotted line and black box). "o" shows the indentation of the cell wall, forming lacunar endocrine gray osmophilic droplets (indicated by the dashed black box).
p: The mature stage is characterized by epithelial cells occupied by large vacuoles, plastids located close to the cell edge, and a remarkable distribution of black osmiophilic droplets in the plastids and vacuoles. The cavity contains a substantial amount of osmophilic compounds.
Black arrow: gray–black osmiophilic droplets
Blue arrows: white vesicles
M: mitochondria
P: chloroplast
G: Golgi apparatus
N: nucleus
V: vacuole
ER: endoplasmic reticulum.

that inwardly depresses and secretes its black osmophilic substance into the cavity (Fig. 3i, j). During the lumen expansion stage (Fig. 2e-g), the lumen is surrounded by 8–10 epithelial cells with a substantial number of osmophilic droplets present between the epithelial cell wall and the plasma membrane (Fig. 3k-o). As lumen expansion progresses, some plastids start to degrade, and osmiophilic droplets within the plastids are transported to the cytoplasm or adjacent endoplasmic reticulum (Fig. 3l). Osmophilic droplets in the cytoplasm either diffuse to the cavity through vesicles (Fig. 3n, o) or are absorbed by the cell wall and subsequently secreted into the cavity through the cup structure for storage (Fig. 3o). Upon maturation of the secretory cavity, the lumen is surrounded by 1–2 layers of flattened epithelial cells and 5–8 layers of sheath cells (Fig. 2h). The epithelial cells contain large vacuoles, whereas the plastids are compressed to the periphery by the vacuoles. These cells do not exhibit obvious osmophilic substances as the primary storage site for these substances is within the cavity itself (Fig. 3p).

3.2. *CgLS is crucial for* D*-limonene synthesis in the secretory cavity of C. grandis 'Tomentosa' fruit*

Two candidate genes (Cg3g004090 and Cg3g004050) were identified through transcriptomics. The *CgLS* (Cg3g004090) and *CgLSX* (Cg3g004050) encode D-limonene synthase. The full-length coding sequence (CDS) of *CgLS* was cloned, comprising 1824 base pairs encoding a protein 607 amino acids long. Comparative analysis of the amino acid sequences of D-limonene synthases from four citrus plants revealed a high degree of similarity (Fig. S1). The Interpro website predicted the conserved regions of *CgLS*, indicating that the CgLS protein contains the Terpene_cyclase_plant_C1 domain associated with the Terpene_cyclase_plant_C1 family (Fig. 4A). Notably, CgLS displayed the conserved motifs RR(X)8 W, DDXXD, and (N, D)D(*L*, *I*, *V*)X(S, T)XXXE (NSE/DTE) from monoterpene synthase (Fig. S1). Phylogenetic analysis demonstrated that CgLS clustered with the terpene synthases from *C. limon*, *C. unshiu*, *C. sinensis*, and *C. japonica* (Fig. 4B), and primarily located in plastids (Fig. 4C). *In vitro* enzyme assays revealed that CgLS could catalyze the conversion of GPP into D-limonene but not FPP (Fig. 5A; Fig. S2). Transient overexpression of *CgLS* markedly induced *CgLS* expression, resulting in a 31 % enhancement of D-limonene synthesis compared to the control group (Fig. 5B). In contrast, TRV-VIGS of *CgLS* in *C. grandis* 'Tomentosa' remarkably suppressed its expression, reducing the D-limonene content by 44.4 % compared to the control group (TRV1 + TRV2) (Fig. 5C). The *CgLSX* (Cg3g004050) gene, comprising 1821 base pairs encoding a protein 606 amino acids long, did not catalyze the substrate GPP and FPP to form any product *in vitro* (Fig. S3).

Furthermore, the expression patterns of *CgLS* at different developmental stages of *C. grandis* 'Tomentosa' fruits were examined, showing an increase as the fruits developed (Fig. 6A). At 30 days after flowering, when the secretory cavity was in the initial cells stage, *CgLS* expression was significantly lower compared to other stages. However, at 180 days after flowering, when the secretory cavity matured, *CgLS* expression was significantly higher (Fig. 6A). Western blotting indicated a similar trend in CgLS content at different developmental stages, corroborating these findings. Specifically, CgLS levels were markedly lower in fruits at 30 days but higher at 60 days compared to other stages (Fig. 6C). Additionally, D-limonene content was lowest at 0.29 mg/g at 30 days but increased dramatically to 12.15 mg/g at 180 days when the fruits reached maturity. Overall, the changes in D-limonene content at different stages exhibited a similar trend to the expression patterns and levels of CgLS.

3.3. *CgLS is synthesized in the endoplasmic reticulum and is predominantly localized to the plastids and vacuoles of secretory cavity cells*

In situ hybridization revealed a prominent expression of *CgLS* in the fruit secretory cavity cells (Fig. 6B). *CgLS* expression signals were specifically detected during the initial cells stage (30 days after flowering) (Fig. 6B-a). Strong signals were observed during the intercellular formation stage (60–90 days after flowering) (Fig. 6B-b). The signal gradually decreased from the lumen expansion stage (Fig. 6B-c, d) to the maturity stage (Fig. 6B-e) (120–180 days after flowering).

Immunohistochemical localization results revealed the expression of CgLS in the fruit secretory cavity cells (Fig. 7). CgLS expression signals were specifically detected during the initial cells stage (Fig. 7D, E). Strong signals were observed during the intercellular formation stage and the lumen expansion stage (Fig. 7F, J, K). The signal was not detected in the maturity stage (Fig. 7).

Immunocytochemical localization was utilized to investigate the spatiotemporal distribution of CgLS during the development of secretory cavity cells. In the early and middle stages of secretory cavity initial cells (Fig. 8a, b), a few anti-CgLS immunogold particles were observed in the endoplasmic reticulum and vacuoles. In the late stage, their number markedly increased, primarily aggregating in the plastids and small

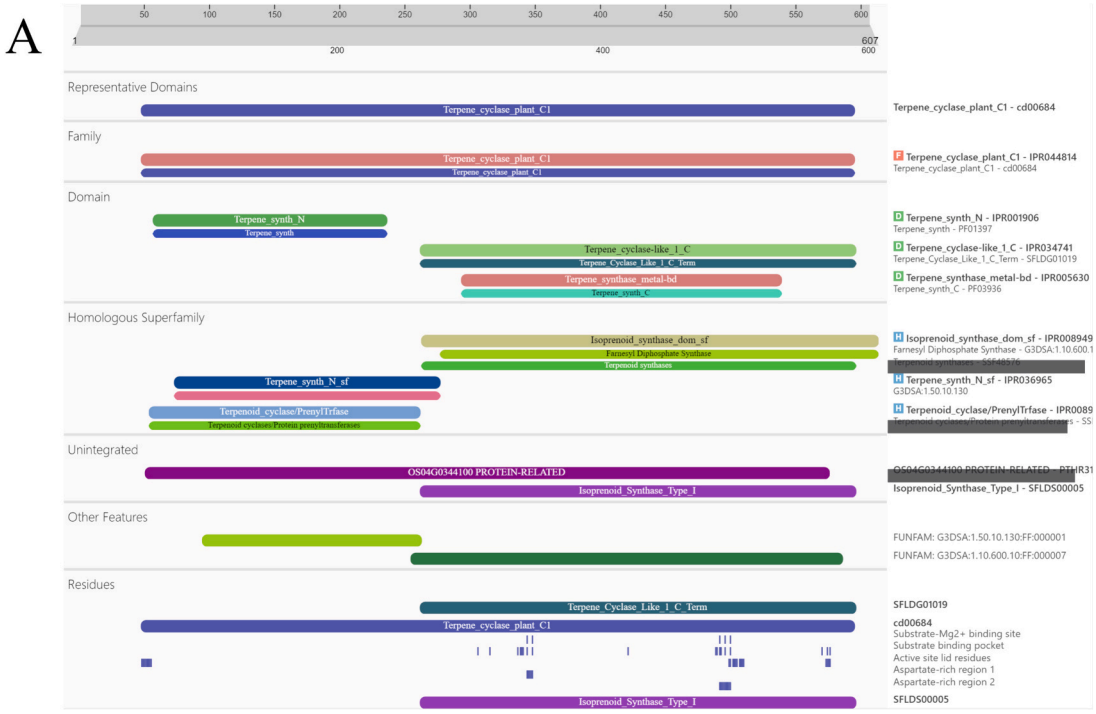

Fig. 4. CgLS sequence analyses and its phylogenetic relationship with TPSs.
A: Prediction of the CgLS functional domain using InterProScan (https://www.ebi.ac.uk/interpro/about/interproscan/).
B: The phylogenetic tree was analyzed using MEGA X (64-bit) (for Windows) for sequence alignment and phylogenetic tree construction. Alignment was by ClustalW (system default parameters). Phylogeny was determined by the Neighor-Joining Tree; test of phylogeny: bootstrap method, no. of bootstrap replications: 500, substitutions type: protein, model/method: p-distance, gaps/missing data treatment: partial deletion, site coverage cut off: 50 %.

The amino acid sequence of CgLS is indicated in red font. The circle in front of the search number indicates its presence in the citrus genus. The green circle is *Citrus sinensis* (XM_006471028.3, XM_025096913.1, XM_006471022.3, XM_024184930.1, KU746814.2, XM_024184526.1,XM_024185200.1, XM_015530477.6); The red circle is *Citrus sinensis* cv. Valencia (Cs3g04170.1, Cs3g04360.1, CS5G22988.1); The blue circle is *Citrus reticulata* (MSYJ216420.1, MSYJ271140.1, MSYJ271160.1); The yellow circle is *Citrus unshiu* (AB110636.1, AB110637.1, AB110640.1, AB110641.1); The black circle is *Citrus limon* (AF514287.1, AF514289.1, AF514286, AF514288); The pink circle is *Citrus jambhiri* (AB266585.1); Other plants are *Murraya paniculata* (HQ636425.1), *Mentha spicata* (L13459.1), *Picea sitchensis* (AY237645.2), *Quercus ilex* (AM283099.1), *Salvia officinalis* (AF051901.1), *Santalum album* (EU798692.1), *Vitis vinifera* (HM807387.1, NM_001281238.1), *Zanthoxylum piperitum* (LC198041.1), *Cinnamomum camphora* (OM721572.1, OM721573.1).

C: CgLS in Tobacco Subcellular Localization. CgLS-eGFP primarily emitted fluorescence in plastids. A small amount of fluorescence was also observed in the cytoplasm adjacent to the plasma membrane. eGFP, GFP channel; Chloroplast, red fluorescence channel; Merge, merged image of eGFP and Chloroplast channels; Bright field, bright-field optical microscopy image; bar = 50 μm.

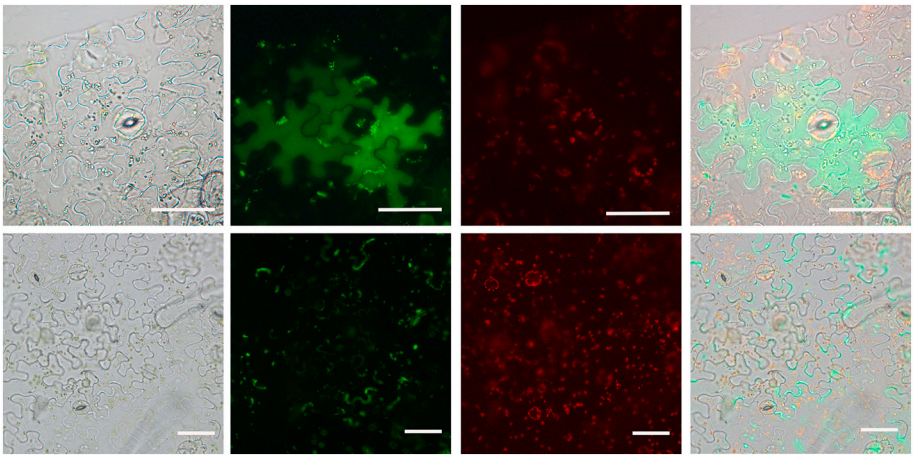

Fig. 4. (*continued*).

vacuoles (Fig. 8c–e). During the intercellular formation stage, most particles were concentrated in the plastids and small vacuoles (Fig. 8f–i). Additionally, a few particles were distributed on the osmophilic droplets within the plastids (Fig. 8g). The small vacuoles containing the particles fused with the large vacuoles (Fig. 8i). As the lumen expanded, the particles were primarily confined to the vacuoles (Fig. 8i–m), while their presence in the plastids decreased significantly (Fig. 8k). The fusion of the small vacuoles containing the immunogold particles with large vacuoles was still evident (Fig. 7m), with the vacuoles exhibiting an abundance of particles (Fig. 8l). At the mature stage, a substantial number of particles were detected in the large vacuole, with only a few in the plastids (Fig. 8n).

4. Discussion

4.1. CgLS is a limonene synthase

Limonene is the simplest cyclic terpene and serves as a synthetic intermediate for many other cyclic terpenes. Thus, LS is a popular model enzyme for studying cyclic monoterpene synthase [42]. The biosynthesis of terpenoids depends on the substrate availability of TPS. In general, monoterpene limonene is synthesized with GPP as a precursor. The first report of cloning the CDS of the LS gene was from *Mentha spicata* L. [43]. The gene was expressed in *Escherichia coli* and the resulting polypeptide, recognized by polyclonal antibodies specific to LS, exhibited the ability to catalyze the *in vitro* synthesis of limonene from GPP, consistent with the function of LS in plants. Maruyama et al. [42] cloned and characterized the D-LS gene (*dLMS*) from *Nepeta cataria* L; both D- and L-LSs shared similar structural features, such as transpeptides, arginine-rich domains, and metal cation binding sites. Lücker [26] isolated two cDNA sequences of (+)-LS genes from the peels of young lemons and expressed the encoded proteins in *E. coli*. D-limonene was the primary product, accompanied by α-pinene, laurene, and sabinene, using GPP as the substrate. Subsequently, a monoterpene synthase gene, *CitMTSE1*, was isolated from *C. unshiu*, and the reactions for determining the *in vitro* enzyme activity of the protein confirmed it to be a D-LS [27]. Monoterpene synthases possess conserved domains, including RRX8W, DDXXD, and NSE/DTE, which are necessary for metal ion binding and separation of the pyrophosphate groups [42,44]. DDXXD is a crucial component of a specific class of synthases, enabling the binding of divalent metal ions (*e.g.*, Mg^{2+}, Mn^{2+}), facilitating and orchestrating their interaction with the phosphate group of the substrate GGP [45]. In our investigation, CgLS possessed the conserved domain of a monoterpene synthase, and the purified protein converted the substrate GPP into D-limonene on the excessive addition of either GPP or FPP. Thus, it can be concluded that CgLS functions as an LS.

4.2. CgLS is involved in D-limonene synthesis in secretory cavity cells of *C. grandis* 'Tomentosa' fruits

Terpenes, particularly monoterpenes with limonene as the main component, are the most volatile compounds found in citrus fruits, closely related to plant defense [46,47]. The essential oil of *C. grandis* 'Tomentosa' (ECG) is rich in limonene (70 %) [13]. However, the limited number of studies on the components of the essential oil from ECG restricts its potential applications [30]. Furthermore, there is a scarcity of research on the regulatory mechanisms underlying its synthesis.

Essential oils are primarily stored in plant secretory structures, such as those found in *Cinnamomum verum* [48], *Arnica* [49], *Magnolia* (*M. zenii* and *M. sirindhorniae*) [50,51], and citrus plants [52–54]. Electron microscopy revealed that the essential oil in ECG was predominantly localized in the secretory cavity cells (Fig. 3), suggesting that it was synthesized and accumulated in the secretory cavity. Previous studies have suggested a close correlation between the synthesis and accumulation patterns of medicinally essential components and the expression profiles of critical regulatory genes within their metabolic pathways [55]. Our research demonstrated a consistent trend among the expression patterns of CgLS, the content of D-limonene, and their development in the fruits (Fig. 6A; Figs. 7, 8). Furthermore, *in situ* hybridization displayed specific expression of CgLS within the secretory cavity (Fig. 6B), indicating that alterations in limonene content were associated with the growth and maturation of the secretory cavity. The collective evidence, supported by both *in vitro* CgLS enzyme activity detection and *in vivo* transient gene overexpression and silencing

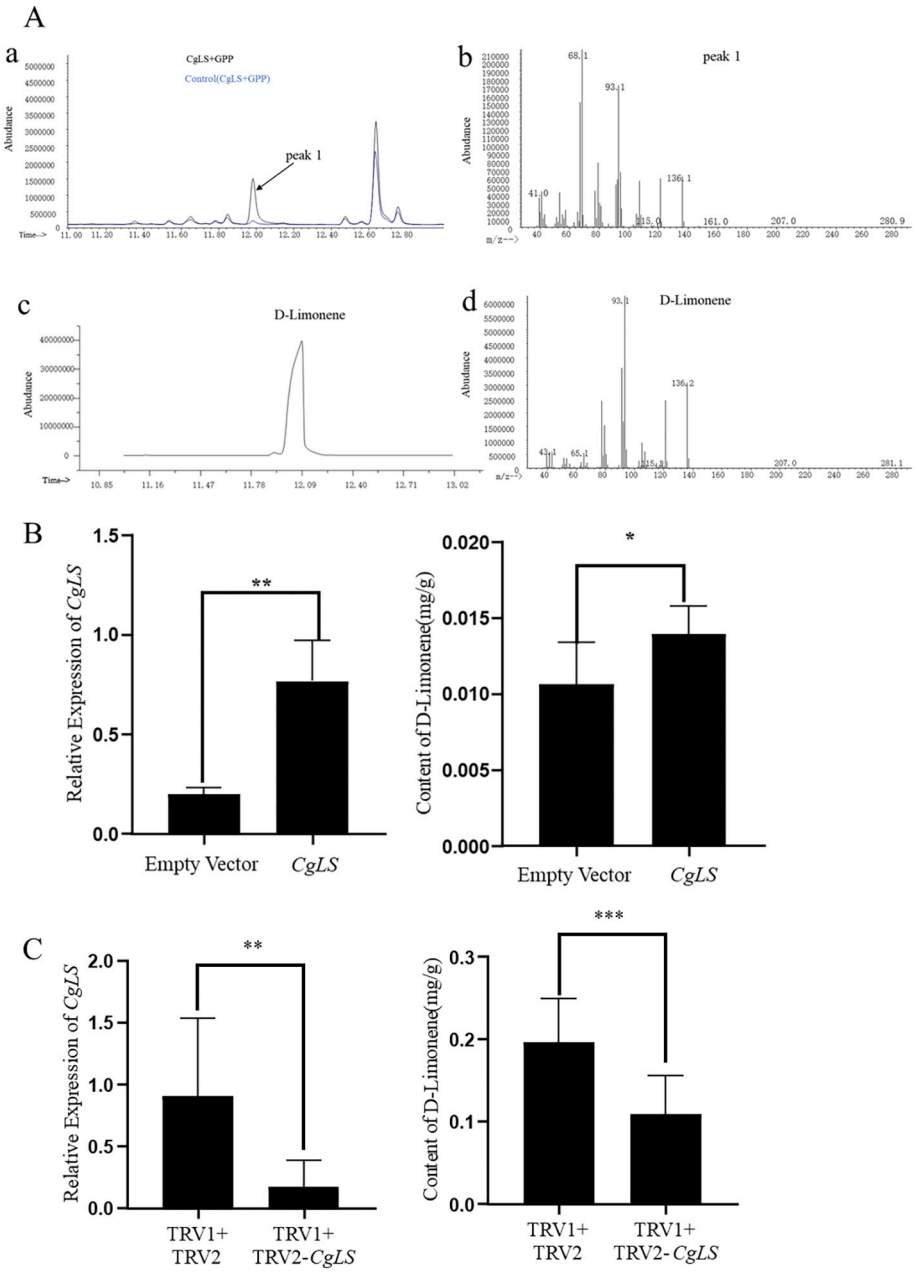

Fig. 5. CgLS catalyzed the *in vitro* and *in vivo* synthesis of D-limonene.
A: The products of the enzyme activity of the CgLS recombinant protein, using GPP as the substrate, were analyzed through GC–MS.
a: A chromatogram of the products of the inactivated CgLS enzyme with the CgLS protein superimposed.
b: The mass spectrum of peak 1 was identified using the NIST14 library.
c: A chromatogram representing the D-limonene standard.
d: The mass spectrum corresponding to the D-limonene standard.
B: Transient overexpression of *CgLS* increased the D-limonene content. The empty vector was used as a control.
C: VIGS silencing of *CgLS* reduced the D-limonene content compared to the TRV1 + TRV2 empty vector control. Significant differences are denoted by asterisks (*$P <$ 0.05; **$P < 0.01$; ***$P < 0.001$).

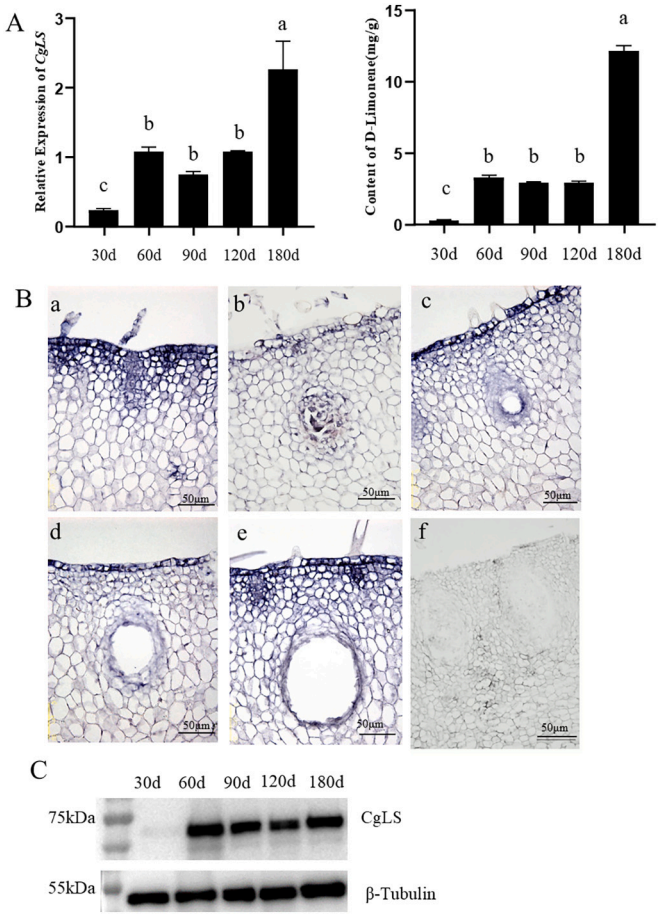

Fig. 6. *CgLS* expression, *in situ* hybridization and Western blot analysis of *C. grandis* 'Tomentosa'e fruit at different development stages.
A: The relative expression of *CgLS* at different developmental stages and the corresponding changes in D-limonene content were examined. The error line represents the standard deviation ($n = 3$), and different letters indicate significant differences at the $P < 0.01$ level.
B: The tissue-specific localization of *CgLS* in the secretory cavity was investigated at different developmental stages using *in situ* hybridization.
a: Initial cells stage
b: Intercellular formation stage
c-d: Lumen expansion stage
e: Mature stage
f: Negative control
C: Western blot analysis of CgLS in different developmental stages.

experiments (Fig. 5), strongly suggested that CgLS plays a direct role in synthesizing D-limonene and regulating its levels within the secretory cavity cells of *C. grandis* 'Tomentosa' fruits.

Terpenoids in plants are primarily synthesized through the MVA pathway in the cytoplasm and the MEP pathway in the plastids [56,57]. However, studies have shown that GPP, FPP, along with their precursors IPP and DMAPP, can shuffle between plastids and cytoplasm *via* yet unrecognized transporters [58–61]. The biosynthesis of monoterpenes in plants is confined to the plastids [62,63], which is attributed to the N-terminal transport peptides in monoterpene synthases [63]. Monoterpene synthases are nucleo-encoded preproteins that undergo proteolytic processing and mature within the plastids [26]. In plants, most monoterpenes are synthesized from the same substrate, GPP, and catalyzed by different monoterpene synthases. GPPS, a short-chain pentenyl transferase, facilitates the condensation of IPP and its isomer DMAPP to produce GPP, the immediate precursor of limonene [64]. The subcellular distribution of GPPSs is crucial in determining the availability of substrates for monoterpene production. The dual targeting of GPPSs to both plastids and cytoplasm affects the synthesis and storage location of monoterpenes in plants [62]. GPPSs in Mentha haplocalyx comprise small subunits (SSU) and large subunits (LSU), both of which possess plastid targeting sequences [65]. Immunocytochemical localization confirmed the presence of GPPSs in the leucoplasts of glandular hair secretory cells in *M. haplocalyx* [29]. Recent findings have indicated that rice OsGPPS and OsGGPPS1, capable of producing GPP and GGPP, are primarily located in the plastids. OsGPS is predominantly responsible for GPP biosynthesis, while OsGGPPS1 can mainly synthesize GGPP [66]. GGPPS isozymes have been identified in the mitochondria, chloroplasts, and endoplasmic reticulum of *Arabidopsis thaliana*, which enable terpene synthases (TPS) to produce monoterpenes by utilizing GPP in the cytoplasm [67,68]. Therefore, the potential dual targeting of GPPSs, coupled with the possible exchange of isoprenoid diphosphate substrates between plastids and cytoplasm, suggests that monoterpene synthesis may not be limited to non-green plastids but can also occur in the cytoplasm.

In this study, anti-CgLS immunogold particles were predominantly found in the plastids and vacuoles, with a smaller proportion in the cytoplasmic matrix. Interestingly, during the early stages of initial cells, these particles accumulated in the endoplasmic reticulum, coinciding with the synthesis of a small amount of D-limonene. Subsequently, from the late early stages of initial cells to the intercellular formation stage, they were distributed in the plastids and vacuoles. This observation aligned with a significant increase in the CgLS levels, indicating a potentially direct utilization of GPP by CgLS in the plastids and vacuoles for D-limonene synthesis, leading to a notable rise in the D-limonene content. As the secretory cavity continued to expand and mature, there was a noteworthy reduction in the accumulation of immunogold particles in the plastids, while their presence was enhanced in the large vacuoles. Concurrently, the production of D-limonene peaked, suggesting an ongoing synthesis of D-limonene catalyzed by CgLS in the vacuole during this period, with the vacuole emerging as the prominent organelle for limonene synthesis in the mature stage. From these observations, it can be inferred that during the initial stages of secretory cavity development, CgLS is synthesized in the endoplasmic reticulum. Subsequently, as the secretory cavity develops, CgLS gradually translocates to the plastids and vacuoles, where it assumes a pivotal role in D-limonene synthesis. In the maturation phase of the fruit, CgLS is predominantly transported to the vacuoles for storage and may continue the synthesis of D-limonene.

5. Conclusion

Our comprehensive transcriptome analysis, combined with *in vitro* and *in vivo* functional verification, has established that CgLS significantly contributes to the synthesis of D-limonene within the secretory cavity cells of *C. grandis* 'Tomentosa' fruits. Cytological, cytochemical, and immunocytochemical investigations demonstrated that CgLS is primarily synthesized in the endoplasmic reticulum of secretory cavity cells and subsequently transported to the plastids and vacuoles for accumulation. These organelles are crucial in utilizing GPP as a substrate for the synthesis and accumulation of D-limonene. Both plastids and vacuoles emerge as major sites for D-limonene synthesis and storage, highlighting the complex intracellular dynamics involved in the metabolic pathway (Fig. 9). This study not only elucidates the pivotal role of CgLS in D-limonene biosynthesis but also provides essential data for further exploration of the regulatory mechanisms and functions of plant terpenoids.

Funding

This work was supported by the Open Competition Program of Ten Major Directions of Agricultural Science and Technology Innovation for the 14th Five-Year Plan of Guangdong Province (No. 2022SDZG07 to H. W.), the National Natural Science Foundation of China (No. 32270381 to MB), the Natural Science Foundation of Guangdong (No.

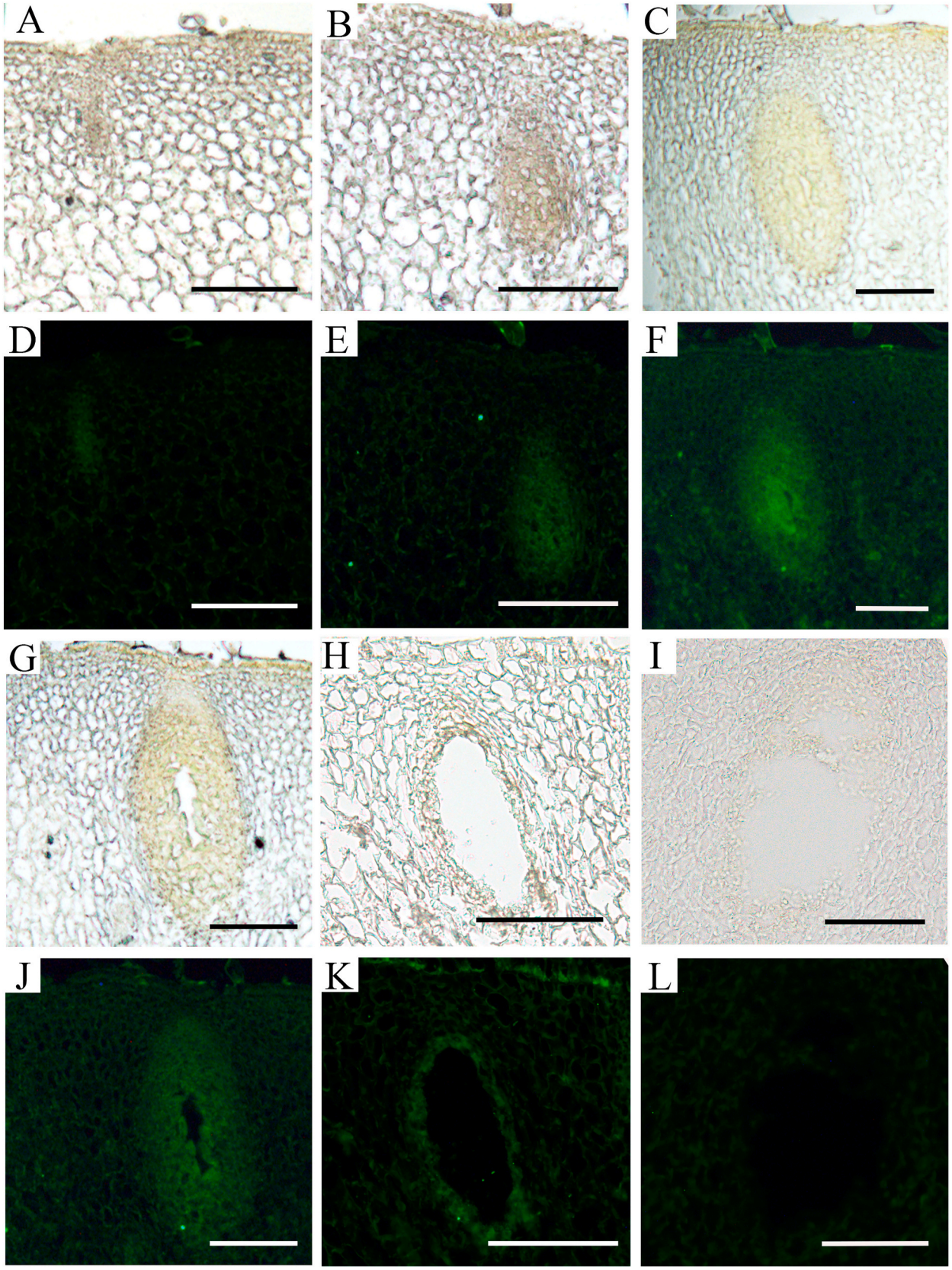

Fig. 7. Immunohistochemical localization of CgLS in the secretory cavities of *C. grandis* 'Tomentosa' fruits at different development stages. A, B, C, G, H, I are bright-field images of the developmental stages of the secretory cavities. D, E, F, J, K, L are the corresponding fluorescence images. I and L: negative controls. A, D: Early stage of initial cells; B: Late stage of s initial cells; C: Intercellular formation stage; G: Lumen expansion stage; H: Maturity stage. Bar = 100 μm.

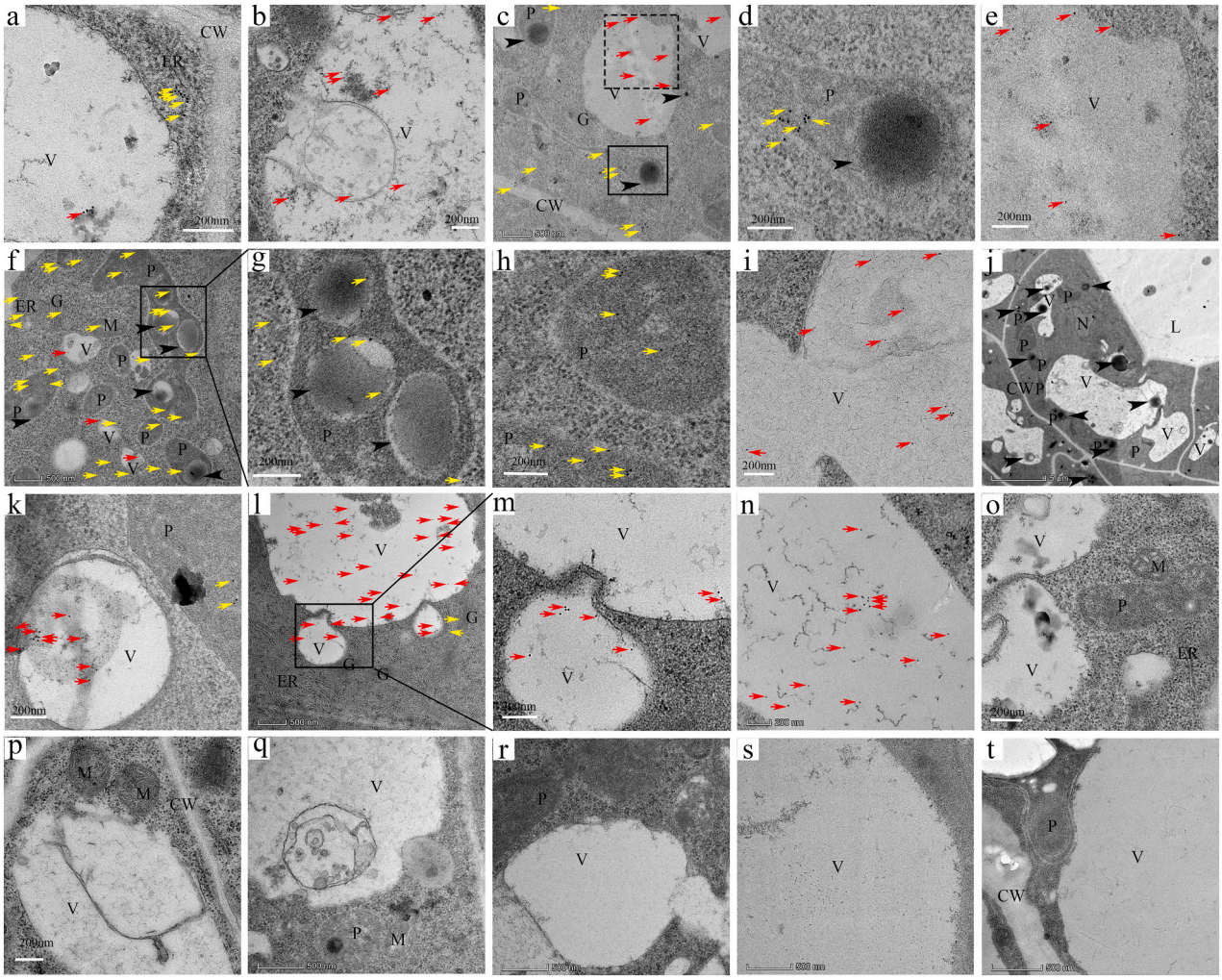

Fig. 8. Immunocytochemical localization of CgLS in the secretory cavities of *C. grandis* 'Tomentosa' fruits at different development stages.
a: In the early stage of initial cells, a few immunogold particles distributed on the endoplasmic reticulum.
b: In the middle stage of initial cells, minuscule amounts of the immunogold particles were distributed in the vacuole.
c–e: In the late stage of initial cells, "d" and "e" correspond to the solid and dotted lines in "c," respectively, indicating the distribution of immunogold particles in the plastids and vacuoles.
f–i: During the intercellular formation stage, "g–h" demonstrates abundant plastids with a large number of gold particles on them. "g" is an enlarged image of the black box in "f," revealing the presence of numerous osmiophilic droplets containing gold particles on the plastids. "i" shows the fusion of vacuoles to form larger ones, enclosing a high concentration of gold particles.
j–m: During the lumen expansion stage, "j" illustrates the first layer of epithelial cells surrounding the lumen. "k" demonstrates gold particles on the plastids. "l" exhibits the numerous gold particles distributed within the enlarged vacuole. "m" is an enlarged image of "l," revealing the accumulation of gold particles in the large vacuole resulting from the fusion of smaller ones.
n: In the mature stage, a large number of gold particles are primarily distributed within the vacuole.
o-t: Negative control. "o": in the early stage of initial cells, "p": in the middle stage of initial cells, "q": during the intercellular formation stage, "r": during the intercellular formation stage, "s": in the mature stage, "t": non-secretory cavity structure.
Black arrow: Gray–black osmiophilic droplets.
CW: Cell wall, ER: Endoplasmic reticulum, P: Plastids, N: Nucleus, V: Vacuoles, G: Golgi apparatus, M: Mitochondria, L: Lumen.
Red arrow: Gold particles are distributed in the vacuole.
Yellow arrow: Gold particles are distributed in plastid, endoplasmic reticulum, cytoplasm and Golgi apparatus.

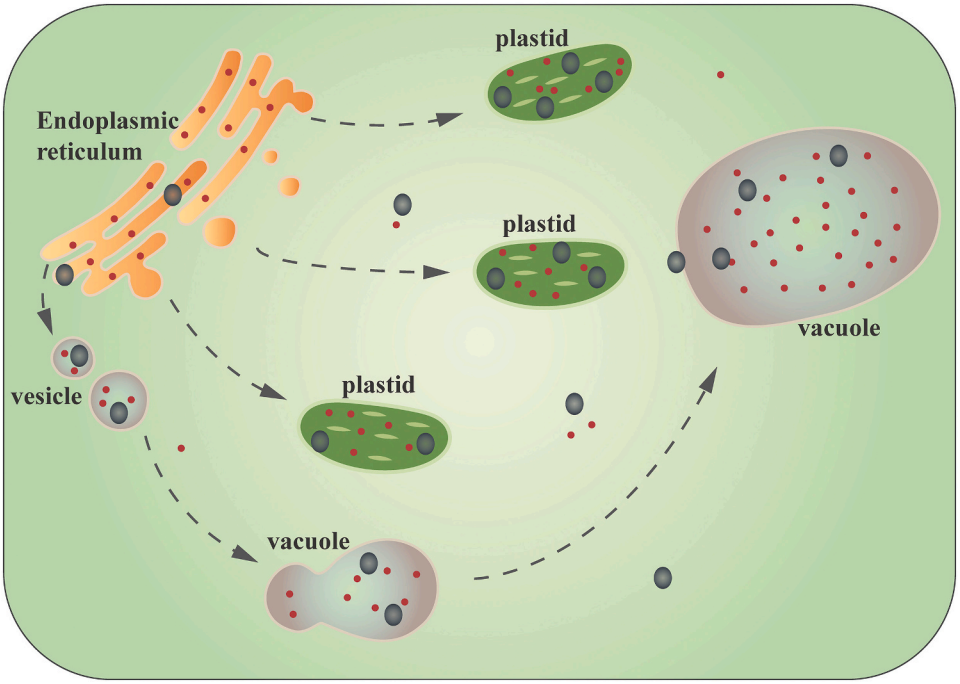

Fig. 9. A model indicating the dynamic changes of CgLS levels in the secretory cavity of *C. grandis* 'Tomentosa' fruits.
Black dots: osmiophilic drops; red dots: CgLS.

2022A1515011086 to MB), the Research Fund of Maoming Branch, Guangdong Laboratory for Lingnan Modern Agriculture (No. 2022KF009 to MB).

CRediT authorship contribution statement

Ning Rong: Formal analysis, Data curation. **Liying Huang:** Data curation. **Peng Ye:** Data curation. **Huimin Pan:** Data curation. **Mingli Hu:** Data curation. **Mei Bai:** Writing – review & editing, Writing – original draft, Project administration, Funding acquisition. **Hong Wu:** Writing – review & editing, Project administration, Investigation, Funding acquisition.

Declaration of competing interest

Authors declare that they have no competing interests. All authors have read and agreed to the published version of the manuscript.

Data availability

All data associated with this paper are provided within the figures and supplementary data published online.

Appendix A. Supplementary data

Supplementary data to this article can be found online at https://doi.org/10.1016/j.ijbiomac.2024.135671.

References

[1] A.K. Maurya, S. Mohanty, A. Pal, C.S. Chanotiya, D.U. Bawankule, The essential oil from *Citrus limetta* Risso peels alleviates skin inflammation: in-vitro and in-vivo study, J. Ethnopharmacol. 212 (2018) 86–94, https://doi.org/10.1016/j.jep.2017.10.018.

[2] H. Bora, M. Kamle, D.K. Mahato, P. Tiwari, P. Kumar, *Citrus* essential oils (CEOs) and their applications in food: an overview, Plants (Basel) 9 (2020) 357, https://doi.org/10.3390/plants9030357.

[3] B. Singh, J.P. Singh, A. Kaur, M.P. Yadav, Insights into the chemical composition and bioactivities of citrus peel essential oils, Food Res. Int. 143 (2021) 110231, https://doi.org/10.1016/j.foodres.2021.110231.

[4] J. Smadja, P. Rondeau, A.S.C. Sing, Volatile constituents of five *Citrus Petitgrain* essential oils from Reunion, Flavour Frag. J. 20 (2005) 399–402, https://doi.org/10.1002/ffj.1438.

[5] L. Soto, G.O.D. Rodriguez, L. Rojas, B. Sulbarán, Chemical characterization of essential oils of grapefruit (*Citrus paradisi* L.), Rev. Fac. Agron. 30 (2013) 266–283.

[6] M. Liu, X. Liu, J. Hu, Y. Xue, X. Zhao, Genetic diversity of limonene synthase genes in Rongan kumquat (*Fortunella crassifolia*), Funct. Plant Biol. 47 (2020) 425–439, https://doi.org/10.1071/FP19051.

[7] A. Smeriglio, L. Cornara, M. Denaro, D. Barreca, B. Burlando, J. Xiao, D. Trombetta, Antioxidant and cytoprotective activities of an ancient Mediterranean citrus (*Citrus lumia* Risso) albedo extract: microscopic observations and polyphenol characterization, Food Chem. 279 (2019) 347–355, https://doi.org/10.1016/j.foodchem.2018.11.138.

[8] M. Mitoshi, I. Kuriyama, H. Nakayama, H. Miyazato, K. Sugimoto, Y. Kobayashi, T. Jippo, K. Kanazawa, H. Yoshida, Y. Mizushina, Effects of essential oils from herbal plants and citrus fruits on DNA polymerase inhibitory, cancer cell growth inhibitory, antiallergic, and antioxidant activities, J. Agric. Food Chem. 60 (2012) 11343–11350, https://doi.org/10.1021/jf303377f.

[9] A. Ben Hsouna, M. Gargouri, W. Dhifi, R.B. Saad, N. Sayahi, W. Mnif, W. Saibi, Potential anti-inflammatory and antioxidant effects of *Citrus aurantium* essential oil against carbon tetrachloride-mediated hepatotoxicity: a biochemical, molecular and histopathological changes in adult rats, Environ. Toxicol. 34 (2019) 388–400, https://doi.org/10.1002/tox.22693.

[10] F. Menichini, M.R. Loizzo, M. Bonesi, F. Conforti, D. De Luca, G.A. Statti, B. de Cindio, F. Menichini, R. Tundis, Phytochemical profile, antioxidant, anti-inflammatory and hypoglycemic potential of hydroalcoholic extracts from Citrus medica L. cv diamante flowers, leaves and fruits at two maturity stages, Food Chem. Toxicol. 49 (2011) 1549–1555, https://doi.org/10.1016/j.fct.2011.03.048.

[11] G. Mitropoulou, E. Fitsiou, K. Spyridopoulou, A. Tiptiri-Kourpeti, H. Bardouki, M. Vamvakias, P. Panas, K. Chlichlia, A. Pappa, Y. Kourkoutas, *Citrus medica* essential oil exhibits significant antimicrobial and antiproliferative activity, LWT Food Sci. Technol. 84 (2017) 344–352, https://doi.org/10.1016/j.lwt.2017.05.036.

[12] E. Jongediar K., M. Buchhaupt, J. Schrader, H. Bouwmeester, J. Beekwilder. Biotechnological production of limonene in microorganisms, Appl. Microbiol. Biotechnol. 100 (2016) 2927–2938, doi:https://doi.org/10.1007/s00253-016-7337-7.

[13] M. Li, H. Chen, C. Liu, J. Guo, X. Xu, H. Zhang, R. Nian, M. Xian, Improvement of isoprene production in Escherichia coli by rational optimization of RBSs and key enzymes screening, Microb. Cell Factories 18 (2019) 4, https://doi.org/10.1186/s12934-018-1051-3.

[14] W.C. West, Ontogeny of oil cells in the woody Ranales, Bull. Torrey. Bot. Club 3 (1969) 329–344, https://doi.org/10.2307/2483738.

[15] R. Maron, A. Fahn, Ultrastructure and development of oil cells in *Laurus nobilis* L. leaves, Bot. J. Linn. Soc. 78 (1979) 31–40, https://doi.org/10.1111/j.1095-8339.1979.tb02184.x.

[16] B.M. Lange, T. Rujan, W. Martin, R. Croteau, Isoprenoid biosynthesis: the evolution of two ancient and distinct pathways across genomes, Proc. Natl. Acad. Sci. USA 97 (2000) 13172–13177.

[17] J. Lombard, D. Moreira, Origins and early evolution of the mevalonate pathway of isoprenoid biosynthesis in the three domains of life, Mol. Biol. Evol. 28 (2011) 87–99, https://doi.org/10.1093/molbev/msq177.

[18] Y. Zhao, M. Wang, Y. Chen, M. Gao, L. Wu, Y. Wang, *LcERF134* increases the production of monoterpenes by activating the terpene biosynthesis pathway in *Litsea cubeba*, Int. J. Biol. Macromol. 232 (2023) 123378, https://doi.org/10.1016/j.ijbiomac.2023.123378.

[19] D.V. Banthorpe, B.V. Charlwood, M.J.O. Francis, Biosynthesis of monoterpenes, Chem. Rev. 25 (1972) 421–424.

[20] L. Dong, E. Jongedijk, H. Bouwmeester, A. Van der Krol, Monoterpene biosynthesis potential of plant subcellular compartments, New Phytol. 209 (2015) 679–690, https://doi.org/10.1111/nph.13629.

[21] A.S. Rai, S.S. Smita, A.K. Singh, K. Shanker, D.A. Nagegowda, Heteromeric and homomeric geranyl diphosphate synthases from *Catharanthus roseus* and their role in monoterpene indole alkaloid biosynthesis, Mol. Plant 6 (2013) 1531–1549, https://doi.org/10.1093/mp/sst058.

[22] H. Wang, D. Ma, J. Yang, An integrative volatile terpenoid profiling and transcriptomics analysis for gene mining and function characterization of AvBPPS and AVTPS1 involved in the monoterpenoid biosynthesis in *Amomum villosum*, Front. Plant Sci. 9 (2018) 846, https://doi.org/10.3389/fpls.2018.00846.

[23] H.M. Kamran, S.B. Hussain, J. Shang, L. Xiang, L.Q. Chen, Identification and molecular characterization of geranyl diphosphate synthase (GPPS) genes in wintersweet flower, Plants 9 (2020) 666, https://doi.org/10.3390/plants9050666.

[24] Y. Zhao, Y. Chen, M. Gao, H. Yin, L. Wu, Y. Wang, Overexpression of geranyl diphosphate *synthase small subunit 1* (*LcGPPS. SSU1*) enhances the monoterpene content and biomass, Ind. Crop. Prod. 143 (2020) 111926, https://doi.org/10.1016/j.indcrop.2019.111926.

[25] G. Beck, D. Coman, E. Herren, M. Águila Ruiz-Sola, M. Rodríguez-Concepción, W. Gruissem, E. Vranová, Characterization of the GGPP synthase gene family in *Arabidopsis thaliana*, Plant Mol. Biol. 82 (2013) 393–416, https://doi.org/10.1007/s11103-013-0070-z.

[26] J. Lücker, M.K. El Tamer, W. Schwab, F.W. Verstappen, L.H. van der Plas, H. J. Bouwmeester, H.A. Verhoeven, Monoterpene biosynthesis in lemon (*Citrus Limon*). cDNA isolation and functional analysis of four monoterpene synthases, Eur. J. Biochem. 269 (2002) 3160–3171, https://doi.org/10.1046/j.1432-1033.2002.02985.x.

[27] T. Shimada, T. Endo, H. Fujii, M. Hara, T. Ueda, M. Kita, M. Omura, Molecular cloning and functional characterization of four monoterpene synthase genes from *Citrus unshiu* Marc, Plant Sci. 166 (2004) 49–58, https://doi.org/10.1016/j.plantsci.2003.07.006.

[28] B.R. Morehouse, R.P. Kumar, J.O. Matos, S.N. Olsen, S. Entova, D.D. Oprain, Functional and structural characterization of a (+)-limonene synthase from *Citrus sinensis*, Biochemistry-US 56 (2017) 1706–1715, https://doi.org/10.1021/acs.biochem.7b00143.

[29] G.W. Turner, R. Croteau, Organization of monoterpene biosynthesis in Mentha. Immunocytochemical localizations of geranyl diphosphate synthase, limonene-6-hydroxylase, isopiperitenol dehydrogenase, and pulegone reductase, Plant Physiol. 136 (2004) 4215–4227, https://doi.org/10.1104/pp.104.050229.

[30] D.L. Su, P.J. Li, S.Y. Que, Z.Q.Y.J. Huang, G.Y. Yuan, Y. Shan Li, Efficient extraction and characterization of pectin from orange peel by a combined surfactant and microwave assisted process, Food Chem. 286 (2019) 1–7, https://doi.org/10.1016/j.foodchem.2019.01.200.

[31] R. Fan, D. Qiu, G. Mao, J. Zeng, Combined analysis of GC-MS, RNA-seq and ATAC-seq elucidates the essential oils variation and terpenes biosynthesis in *Citrus*, Ind. Crop. Prod. 209 (2024) 117996, https://doi.org/10.1016/j.indcrop.2023.117996.

[32] A.J. Vieira, F.P. Beserra, M.C. Souza, A.L. Rozza, Limonene: aroma of innovation in health and disease, Chem. Biol. Interact. 283 (2018) 97–106, https://doi.org/10.1016/j.cbi.2018.02.007.

[33] X. Huang, X. Li, Q. Qin, Y. Li, W. Zhang, H. Tang, Anti-inflammatory and antinociceptive effects of active ingredients in the essential oils from *Gynura procumbens*, a traditional medicine and a new and popular food material, J. Ethnopharmacol. 239 (2019) 111916, https://doi.org/10.1016/j.jep.2019.111916.

[34] F.R. Pinheiro-Neto, E.M. Lopes, B.T. Acha, L.D.S. Gomes, W.A. Dias, A.C.D. Reis Filho, B.S. Leal, D.C.D.N. Rodrigues, J.D.N. Silva, D. Dittz, P.M.P. Ferreira, F.R. C. Almeida, α-Phellandrene exhibits antinociceptive and tumor-reducing effects in a mouse model of oncologic pain, Toxicol. Appl. Pharmacol. 418 (2021) 115497, https://doi.org/10.1016/j.critrevonc.2015.12.011.

[35] E.W.M. Pereira, L.H. Heimfarth, T.K.B. Santos, F.R.S. Passos, P. Siqueira-Lima, L. Scotti, M.T. Scotti, J.R.G. da Silva Almeida, A.R. Campos, H.D.M. Coutinho, P. Martin, L.J. Quintans-Júnior, J.S.S. Quintans, Limonene, a citrus monoterpene, non-complexed and complexed with hydroxypropyl-β-cyclodextrin attenuates acute and chronic orofacial nociception in rodents: evidence for involvement of the PKA and PKC pathway, Phytomedicine 96 (2022) 53893, https://doi.org/10.1016/j.phymed.2021.153893.

[36] M. Bai, M. Liang, B. Huai, H. Gao, P. Tong, R. Shen, H. He, H. Wu, Ca^{2+}-dependent nuclease is involved in DNA degradation during the programmed cell death of secretory cavity formation in *Citrus grandis* 'Tomentosa' fruits, J. Exp. Bot. 71 (2020) 4812–4827, https://doi.org/10.1093/jxb/eraa199.

[37] L. Xian, S.K. Sahu, L. Huang, Y. Fan, J. Lin, J. Su, M. Bai, Y. Chen, S. Wang, P. Ye, F. Wang, Q. Luo, H. Bai, X. Lin, C. Yuan, X. Geng, H. Liu, H. Wu, The draft genome and multi-omics analyses reveal new insights into geo-herbalism properties of *Citrus grandis* 'Tomentosa', Plant Sci. 325 (2022) 111489 https://doi.org/10.1016/j.plantsci.2022.111489.

[38] X. Li, Y. Xu, S. Shen, X. Yin, H. Klee, B. Zhang, K. Chen, R. Hancock, Transcription factor CitERF71 activates the terpene synthase gene CitTPS16 involved in the synthesis of E-geraniol in sweet orange fruit, J. Exp. Bot. 68 (2017) 4929–4938, https://doi.org/10.1093/jxb/erx316.

[39] Q. Wang, X.Q. Huang, T.J. Cao, Z. Zhuang, R. Wang, L. Shan, Heteromeric geranylgeranyl diphosphate synthase contributes to carotenoid biosynthesis in ripening fruits of red pepper (*Capsicum annuum* var. *conoides*), J. Agric. Food Chem. 66 (2018) 11691–11700, https://doi.org/10.1021/acs.jafc.8b04052.

[40] X.R. Yin, X.L. Xie, X.J. Xia, J.Q. Yu, I.B. Ferguson, J.J. Giovannoni, K.S. Chen, Involvement of an ethylene response factor in chlorophyll degradation during citrus fruit degreening, Plant J. 86 (2016) 403–412, https://doi.org/10.1111/tpj.13178.

[41] J. Wen, Y. Wang, X. Lu, H. Pan, D. Jin, J. Wen, C. Jin, S.K. Sahu, J. Su, X. Luo, X. Jin, J. Zhao, H. Wu, E. Liu, H. Liu, An integrated multi-omics approach reveals polymethoxylated flavonoid biosynthesis in *Citrus reticulata* cv. Chachiensis, Nat. Commun. 15 (2024) 3991, https://doi.org/10.1038/s41467-024-48235-y.

[42] T. Maruyama, M. Ito, F. Kiuchi, G. Honda, Molecular cloning, functional expression and characterization of d-limonene synthase from *Schizonepeta tenuifolia*, Biol. Pharm. Bull. 4 (2002) 373–377, https://doi.org/10.1248/bpb.25.661.

[43] S.M. Colby, W.R. Alonso, E.J. Katahira, D.J. McGarvey, R. Croteau, 4S-limonene synthase from the oil glands of spearmint (*Mentha spicata*). cDNA isolation, characterization, and bacterial expression of the catalytically active monoterpene cyclase, J. Biol. Chem. 31 (1993) 23016–23024, https://doi.org/10.1016/S0021-9258(19)49419-2.

[44] N. Srividya, E.M. Davis, R.B. Croteau, B.M. Lange, Functional analysis of (4S)-limonene synthase mutants reveals determinants of catalytic outcome in a model monoterpene synthase, Proc. Natl. Acad. Sci. USA 112 (2015) 3332–3337, https://doi.org/10.1073/pnas.1501203112.

[45] C.A. Lesburg, G. Zhai, D.E. Cane, Crystal structure of pentalenene synthase: mechanistic insights on terpenoid cyclization reactions in biology, Science 277 (1997) 1820–1824.

[46] S.M. Abd-Elwahab, N.D. El-Tanbouly, M.Y. Moussa, A.R. Abdel-Monem, N. M. Fayek, Antimicrobial and antiradical potential of four agro-waste *Citrus* peels cultivars, J. Essent. Oil Bear. Pl. 19 (2016) 1932–1942, https://doi.org/10.1080/0972060X.2016.1232609.

[47] L. GUO, H. Yao, W. Chen, X. Wang, P. Ye, Z. Xu, S. Zhang, H. Wu. Natural products of medicinal plants: biosynthesis and bioengineering in post-genomic era. Hortic. Res. 9 (2022) 223, doi:https://doi.org/10.1093/hr/uhac223.

[48] Y. Li, D. Kong, X. Lin, Z. Xie, M. Bai, S. Huang, H. Nian, H. Wu, Quality evaluation for essential oil of *Cinnamomum verum* leaves at different growth stages based on GC–MS, FTIR and microscopy, Food Anal. Mothod. 9 (2015) 202–212, https://doi.org/10.1007/s12161-015-0187-6.

[49] K. Kromer, A. Kreitschitz, T. Kleinteich, S.N. Gorb, A. Szumny, Oil secretory system in vegetative organs of three Arnica taxa: essential oil synthesis, distribution and accumulation, Plant Cell Physiol. 57 (2016) 1020–1037, https://doi.org/10.1093/pcp/pcw040.

[50] M.L. Hu, Y.mQ. Li, M. Bai, Y. L. Wang, H. Wu., Variations in volatile oil yields and compositions of *Magnolia zenii* Cheng flower buds at different growth stages, Trees-Struct. Funct. 29 (2015) 1649–1660, https://doi.org/10.5650/jos.ess17229.

[51] D. Ghosh, N. Chaudhary, K. Uma Kumari, J. Singh, P. Tripathi, A.S. Meena, A. Yadav Luqman, C.S. Chanotiya, G. Pandey, N. Kumar, Diversity of Essential oil-secretory cells and oil composition in flowers and buds of *Magnolia sirindhorniae* and its biological activities, Chem. Biodivers. 18 (2021) e2000750, https://doi.org/10.1002/cbdv.202000750.

[52] M.M. Ahmad, Anjum F.M. Salim-ur-Rehman, E.E. Bajwa, Comparative physical examination of various citrus peel essential oils, Int. J. Agric. Biol. 8 (2006) 186–190.

[53] S. Liang, H. Wang, M. Yang, H. Wu, Sequential actions of pectinases and cellulases during secretory cavity formation in *Citrus* fruits, Trees-Struct. Funct. 1 (2009) 19–27, https://doi.org/10.1007/s00468-008-0250-7.

[54] P.P. Tong, B. Huai, Y. Chen, M. Bai, H. Wu, CisPG21 and CisCEL16 are involved in the regulation of the degradation of cell walls during secretory cavity cell programmed cell death in the fruits of *Citrus sinensis* (L.) Osbeck, Plant Sci. 297 (2020) 3222, https://doi.org/10.1016/j.plantsci.2020.110540.

[55] Y. Li, D.X. Kong, R.S. Huang, H.L. Liang, G.G. Xu, H. Wu, Variations in essential oil yields and compositions of cinnamomum cassia leaves at different developmental stages, Ind. Crop. Prod. 47 (2013) 92–101, https://doi.org/10.1016/j.indcrop.2013.02.031.

[56] J. Chappell, The biochemistry and molecular biology of isoprenoid metabolism, Plant Physiol. 107 (1995) 1–6, https://doi.org/10.1104/pp.107.1.1.

[57] B.M. Lange, S.S. Mahmoud, M.R. Wildung, G.W. Turner, E.M. Davis, I. Lange, R. C. Baker, R.A. Boydston, R.B. Croteau, Improving peppermint essential oil yield and composition by metabolic engineering, Proc. Natl. Acad. Sci. USA 108 (2011) 16944–16949, https://doi.org/10.1073/pnas.1111558108.

[58] E. Soler, M. Clastre, B. Bantignies, C. Ambid, Uptake ofisopentenyl diphosphate by plastids isolated from *Vitis vinifera* L. cell suspensions, Planta 91 (1993) 324–329, https://doi.org/10.1007/BF00195689.

[59] N. Nagata, M. Suzuki, S. Yoshida, T. Muranaka, Mevalonic acid partially restores chloroplast and etioplast development in lacking the non-mevalonate pathway, Planta 216 (2002) 345–350, https://doi.org/10.1007/s00425-002-0871-9.

[60] M. Gutensohn, I. Orlova, T.T.H. Nguyen, R. Davidovich-Rikanati, M.G. Ferruzzi, Y. Ferzzi, E. Lewinsohn, E. Pichersky, N. Dudareva, Cytosolic monoterpene biosynthesis is supported by plastid-generated geranyl diphosphate substrate in transgenic tomato fruits, Plant J. 75 (2013) 351–363, https://doi.org/10.1111/tpj.12212.

[61] E. Vranová, D. Coman, W. Gruissem, Network analysis of the MVA and MEP pathways for isoprenoid synthesis, Annu. Rev. Plant Biol. 64 (2013) 665–700, https://doi.org/10.1146/annurev-arplant-050312-120116.

[62] F. Bouvier, C. Suire, A. d'Harlingue, B. Backhaus, B. Camara, Molecular cloning of geranyl diphosphate synthase and compartmentation of monoterpene synthesis in plant cells, Plant J. 24 (2000) 241–252, https://doi.org/10.1046/j.1365-313x.2000.00875.x.

[63] M. Borghi, D.Y. Xie, Cloning and characterization of a monoterpene synthase gene from flowers of Camelina sativa, Planta 247 (2018) 443–457, https://doi.org/10.1007/s00425-017-2801-x.

[64] D. Tholl, C.M. Kish, I. Orlova, D. Sherman, J. Gerhenzon, E. Pichersky, N. Dudareva, Formation of monoterpenes in Antirrhinum majus and Clarkia breweri flowers involves heterodimeric geranyl diphosphate synthases, Plant Cell 16 (2004) 977–992, https://doi.org/10.1105/tpc.020156.

[65] C.C. Burke, M.R. Wildung, R. Croteau, Geranyl diphosphate synthase: cloning, expression, and characterization of this prenyltransferase as a heterodimer, Proc. Natl. Acad. Sci. USA 96 (1999) 13062–13067, https://doi.org/10.1073/pnas.96.23.13062.

[66] M.K. You, Y.J. Lee, J.S. Yu, S.H. Ha, The predicted functional compartmentation of rice terpenoid metabolism by *trans*-prenyltransferase structural analysis, expression and localization, Int. J. Mol. Sci. 21 (2020) 8927, https://doi.org/10.3390/ijms21238927.

[67] K. Okada, T. Saito, T. Nakagawa, M. Kawamukai, Y. Kamiya, Five geranylgeranyl diphosphate synthases expressed in different organs are localized into three subcellular compartments in Arabidopsis, Plant Physiol. 122 (2000) 1045–1056, https://doi.org/10.1104/pp.122.4.1045.

[68] I. Thabet, G. Guirimand, A. Guihur, A. Lanoue, V. Courdavault, N. Papon, S. Bouzid, N. Giglioli-Guivarc'h, A.J. Simkin, M. Clastre, Characterization and subcellular localization of geranylgeranyl diphosphate synthase from *Catharanthus roseus*, Mol. Biol. Rep. 39 (2012) 3235–3243, https://doi.org/10.1007/s11033-011-1091-9.